Journal of Chromatography A, 1218 (2011) 2405–2412

Contents lists available at ScienceDirect

Journal of Chromatography A

journal homepage: www.elsevier.com/locate/chroma

Chromatographic behavior of IgM:DNA complexes

Pete Gagnon[a,*], Frank Hensel[b], Soon Lee[c], Simin Zaidi[c]

[a] Bioprocessing Technology Institute, 20 Biopolis Way, 06-01 Centros, Singapore 138668
[b] Patrys GmbH, Friedrich-Bergius Ring 15, D-97076 Wuerzburg, Germany
[c] Avid Bioservices, 14282 Franklin Avenue, Tustin, CA 92780, USA

ARTICLE INFO

Article history:
Available online 23 December 2010

Keywords:
IgM
DNA
Complexes
Purification
Monoliths

ABSTRACT

This study documents the presence of stable complexes between monoclonal IgM and genomic DNA in freshly harvested mammalian cell culture supernatants. 75% of the complex population elutes from size exclusion chromatography with the same retention volume as IgM. DNA comprises 24% of the complex mass, corresponding to an average of 347 base pairs per IgM molecule, distributed among fragments smaller than about 115 base pairs. Electrostatic interactions appear to provide most of the binding energy, with secondary stabilization by hydrogen bonding and metal affinity. DNA-dominant complexes are unretained by bioaffinity chromatography, while IgM-dominant complexes are retained and coelute with IgM. DNA-dominant complexes are repelled from cation exchangers, while IgM-dominant complexes are retained and partially dissociated. Partially dissociated forms elute in order of decreasing DNA content. The same pattern is observed with hydrophobic interaction chromatography. All complex compositions bind to anion exchangers and elute in order of increasing DNA content. A porous particle anion exchanger was unable to dissociate DNA from IgM. Monolithic anion exchangers, offering up to15-fold higher charge density, achieved nearly complete complex dissociation. The charge-dense monolith surface appears to outcompete IgM for the DNA. Monoliths also exhibit more than double the IgM dynamic binding capacity of the porous particle anion exchanger, apparently due to better surface accessibility and more efficient mass transfer.

1. Introduction

IgM monoclonal antibodies are candidates for an increasing number of important healthcare applications including cancer therapy [1–4], treatment of infectious disease [5], AIDS vaccine [6], and reagents for characterizing stem cell differentiation [7,8]. Their unique effectiveness is due largely to their ability to discriminate glycosylation variants on key antigens that are either unrecognized or poorly recognized by IgG. Ongoing successful clinical trials demonstrate that human-injectable quality IgM can be prepared on an industrial scale [5] but purification concerns linger for this antibody class overall. They can be purified by a variety of precipitation and chromatography methods [7–10], but have a tendency to form nonspecific complexes with DNA [11,12]. Such complexes are sufficiently stable that immobilized DNA has been used effectively as an affinity ligand for IgM purification [12]. This warns of potential to form stable complexes during cell culture production, that could impair the ability of commonly used purification methods to reduce DNA to clinically acceptable levels.

Experimental data demonstrating that antibody:contaminant complexes depress the effectiveness of purification methods were published recently by Shukla et al., whose results showed that more than 95% of the host cell protein contaminants carried through protein A affinity chromatography were complexed to IgG during cell culture production [13]. Subsequent work by Luhrs et al. has shown that core histones and DNA ejected from dead cells participate in the formation of complexes with IgG [14]. If not addressed by special measures during purification, these contaminants are carried along as "hitchhikers" in the final product, imposing elevated background interference in assays, even to the point of producing false positive test results. This creates an obvious concern for therapeutic applications as well.

The present study provides baseline data on the composition and chromatographic behavior of IgM:DNA complexes. Naturally occurring complexes from cell culture supernatant are isolated by a combination of hydroxyapatite (HA) and anion exchange chromatography (AX), then their retention behavior characterized by size exclusion (SEC), AX, cation exchange (CX), hydrophobic interaction (HIC), and bioaffinity chromatography (AC). Experiments are conducted over a range of pH and conductivity values, and at various urea concentrations. Consideration is given to the mechanisms potentially involved in complexation. Practical ramifications for purification of IgM and other biopharmaceuticals are discussed.

* Corresponding author. Tel.: +65 6407 0941; fax: +65 6478 9561.
E-mail address: pete_gagnon@bti.a-star.edu.sg (P. Gagnon).

0021-9673/$ – see front matter © 2011 Elsevier B.V. All rights reserved.
doi:10.1016/j.chroma.2010.12.066

2. Materials and methods

2.1. Chromatography instrumentation and media

All chromatography experiments were conducted on an AKTA™ Explorer 100 (GE Healthcare). 0.34 mL axial flow monolithic anion exchangers (CIM® QA, EDA) and a strong cation exchanger (CIM SO3) were obtained from BIA Separations (Klagenfurt, Austria). A porous particle anion exchanger, Fractogel® TMAE HiCap, was obtained from EMD Biosciences (Gibbstown, NJ, USA). Experimental wide pore weakly hydrophobic media (PPG Toyopearl® HW75) was obtained from Tosoh BioScience (King of Prussia, PA, USA). Ceramic hydroxyapatite CHT™ type II, 40 μm was obtained from Bio-Rad Laboratories (Hercules, CA, USA). Immobilized anti-lambda light chain camelid VHH (CaptureSelect™ Lambda Fab) was obtained from BAC (Leiden, NL). A 7.8 mm × 30 cm TSKgel® G5000PWXL-CP analytical SEC column was obtained from Tosoh Bioscience. Buffer components were obtained from Sigma/Aldrich (St. Louis, MO, USA). All buffers were prepared with water for injection (WFI) and filtered to 0.22 μm prior to use.

2.2. Preparation of IgM, DNA, and complexes

Purified genomic DNA (gDNA) from salmon sperm was obtained from Sigma, dissolved to a final concentration of 0.1 mg/mL in 25 mM Hepes, pH 7.0, and filtered to 0.22 μm. Purified DNA-depleted monoclonal IgM was obtained as described in [10]. In brief, IgM was eluted from HA with a linear gradient from 10 to 500 mM sodium phosphate, pH 7.0. The IgM pool from HA was applied to a QA AX monolith and eluted with a linear gradient to 1 M sodium chloride (50 mM Hepes, pH 7.0). The IgM pool from AX was applied to a SO3 CX monolith and eluted with a linear gradient to 500 mM sodium chloride (50 mM Hepes, pH 7.0). IgM prepared in this manner was greater than 99% pure, contained less than 0.5% aggregates, with DNA levels below 1 part per million (ppm, qPCR performed by BioReliance, Rockville, MD) [15].

Naturally occurring IgM:DNA complexes were isolated from IgM-containing hybridoma cell culture supernatant (CCS) by a combination of HA and AX. 8 L of filtered CCS was applied to a 400 mL HA column (XK50, GE Healthcare, 200 cm/h) and eluted as described above. The IgM peak was applied to a 110 mL column of Fractogel TMAE HiCap (XK26, GE Healthcare, 200 cm/h) and eluted with a linear gradient to 1 M NaCl (20 mM Tris, pH 8.0). Fractions were analyzed by reduced SDS PAGE. IgM and DNA peaks were set aside. Intermediate fractions containing complexes were pooled for additional study. Creation of artificial IgM:DNA complexes was attempted by addition of purified gDNA to purified IgM to provide an experimental control, but resulted in immediate formation of a dense white insoluble precipitate.

2.3. Estimation of IgM and DNA

Relative IgM:DNA levels within chromatography experiments were estimated by comparing UV absorbance at 254 and 280 nm. 254 nm was used for DNA instead of the usual 260 because 254 supports nearly equivalent DNA absorbance but occurs at a protein absorbance minimum that supports better differentiation of protein from DNA. IgM gave 254/280 ratios of about 0.5. DNA gave a 254/280 ratio of about 2.0. This enabled visual estimation of relative DNA levels directly from chromatograms. More precise proportioning was calculated with the equation developed by Warburg [16].

$$A254/280 = \frac{(e254_P \times (\%P) + e254_N \times (\%N))}{(e280_P \times (\%P) + e280_N \times (\%N))}$$

where e = the extinction coefficient; P = protein, and N = nucleotide.

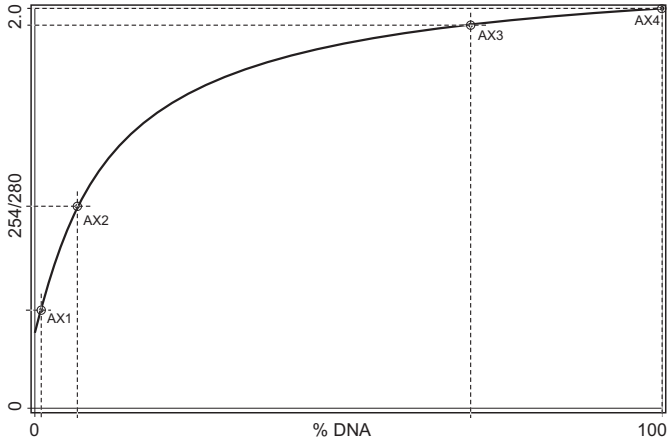

Fig. 1. Warburg plot of DNA to protein mass based on UV absorbance at 254 and 280 nm, calculated from the equation and extinction coefficients given in Section 2. The nonlinearity of the plot results from the fact that DNA absorbs 8.5 times more UV at 280 nm than IgM. AX1–AX4 refer to fractions from the anion exchange experiment illustrated in Fig. 2.

The extinction coefficients for IgG and IgM at 254 were 0.45; at 280, IgG 1.4, IgM 1.18 [17]. Extinction coefficients for IgG and IgM at 254 nm were derived from comparison of the absorbance of purified protein at 254 and 280 nm. The extinction coefficient for DNA at 254 was 20; at 280, 10. Fig. 1 illustrates the curve generated by this equation, from which the mass ratio of DNA to IgM can be determined easily. While convenient, the accuracy of this method suffers from the disproportionately high 280 absorbance of DNA [18–20]. It is also variable with respect to conductivity and pH [21].

Protein concentration of the complex pool employed in the majority of experiments was estimated by Micro BCA assay, performed according to manufacturer's instructions (Pierce Chemical Company, Rockford, IL). DNA concentration was estimated by qPCR. DNA was extracted in triplicate using a PrepSEQ Residual DNA Sample Preparation Kit from Applied Biosystems (Carlsbad, CA), and measured by amplification of an 18S rRNA gene fragment. Primers for *Mus musculus* 18S rRNA were synthesized by Integrated DNA Technologies (Coralville, IA). A standard curve was developed with NS0 mouse myeloma genomic DNA, prepared with a Qiamp DNA Mini and Blood Mini Kit (Qiagen, Valencia, CA), with additional cleaning by a Genomic DNA Clean and Concentrator Kit (Zymo Research, Orange, CA). Real-time PCR was performed using an icycler iQ5 (BioRad).

2.4. Size exclusion chromatography

Analytical SEC was conducted in a buffer of 50 mM MES, 200 mM arginine, 300 mM NaCl, 10 mM EDTA, pH 6.5, intended to preemptively suppress nonspecific interactions between sample components and the solid phase [22]. Sample volume was 0.5 mL. Volumetric flow rate was 0.25 mL/min (linear flow rate 31.4 cm/h).

2.5. Affinity chromatography

AC was conducted on a 1 mL (5 mm× 50 mm) Lambda column. The column was equilibrated with 50 mM Hepes, 100 mM NaCl, pH 7.0 (HBS) at a volumetric flow rate of 1 mL/min (linear, 300 cm/h). The first experiment was conducted with sample from the TMAE pool, at about 300 mM NaCl. In the second experiment, NaCl was added to the flow-through from the first experiment to a final concentration of about 1.5 M, and applied to the column. In the third experiment, NaCl was added to the flow-through from the second experiment to a final concentration of about 3.0 M, and applied to the column. After loading, the column was washed with HBS, fol-

lowed by a second wash with 2 M urea, 1.5 M NaCl, 10 mM EDTA, buffer, pH 7.0. The column was washed again with HBS then eluted with 500 mM arginine, 50 mM MES, pH 5. The column was regenerated with 2 M guanidine, pH 5.5 after each run.

2.6. Hydrophobic interaction chromatography

HIC was conducted on a 1 mL (5 mm × 50 mm) column equilibrated with 50 mM Hepes, 1.0 M ammonium sulfate, pH 7.0, at a volumetric flow rate of 1 mL/min (linear, 300 cm/h). Sample was prepared by adding NaCl to the TMAE complex pool, to a final concentration of 3.2 M. This composition was found to achieve good binding of purified DNA-free IgM, and was advantageous to equilibrating the sample with ammonium sulfate, since the latter caused the sample to precipitate prior to column loading. Sample was loaded, the column washed with equilibration buffer then eluted in a 15 column volume (CV) linear gradient ending in 50 mM Hepes, pH 7.0. The column was regenerated with 2 M guanidine, pH 5.5 after each run.

2.7. Cation exchange chromatography

Experiments were run on a single 334 μL CIM SO3 disk at a flow rate of 4 mL/min. Sample was prepared by diluting the TMAE complex pool 1:9 with 20 mM MES, pH 6. The monolith was equilibrated with the same buffer or with 20 mM Hepes, pH 7.0; loaded; washed with equilibration buffer then eluted with a linear gradient to 0.5 M NaCl in the same buffer and pH. The column was regenerated with 2 M guanidine, pH 5.5 after each run.

2.8. Anion exchange chromatography

Analytical and dynamic capacity experiments were performed on a 1 mL (5 mm × 50 mm, porous particle) column of TMAE HiCap at 300 cm/h. Monolithic experiments were run on a single 334 μL CIM QA or EDA disk at a flow rate of 4 mL/min. For some experiments, 3 monolithic disks were stacked in a single housing to yield a total media volume of 1 mL, run at 1 mL/min. Sample was prepared by diluting the TMAE complex pool from section 2.2 1:9 with 20 mM Tris, pH 8.0. Experiments were conducted on monoliths at pH 6.0, 7.0, and 8.0, buffering with 20 mM MES, Hepes, or Tris, respectively. Columns were equilibrated, loaded, washed, then eluted with linear gradients to 2 M NaCl in the same base buffer, except as noted otherwise. Columns were regenerated with 2 M guanidine, pH 5.5 after each run.

The effects of DNA:IgM complexes on AX binding capacity were assessed in a series of experiments, applying 0.14, 1.4, and 14 mg of complex (expressed here as protein mass only) to a 1-mL stack of 3 EDA monoliths. Dynamic capacity of purified DNA-depleted IgM was measured as described in [10]. In brief, the columns being evaluated were equilibrated to loading conditions and taken off line. IgM feed was then run through the chromatograph until UV absorbance achieved a constant value. This value represented 100% breakthrough. The first column was put back in-line, dropping UV absorbance to zero, and UV monitored until 10% breakthrough was achieved, then the next column was placed in line; then the next. Dynamic binding capacities were calculated by multiplying feed concentration by the volume of feed applied up to 5% breakthrough.

Other experimental details and variations are described in the following sections.

3. Results and discussion

3.1. Characterization of IgM:DNA complexes

Fig. 2 illustrates the chromatogram of the TMAE experiment by which complexes were isolated to conduct this study. The

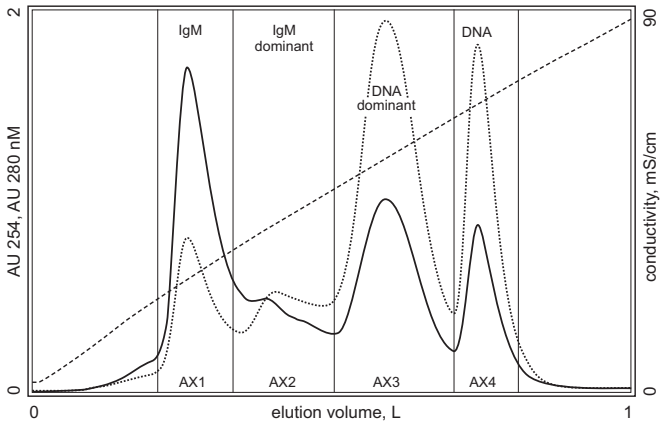

Fig. 2. Anion exchange fractionation of IgM, DNA, and complexes on TMAE HiCap. The feed stream was the IgM-containing fraction from hydroxyapatite eluted with a phosphate gradient. The solid black line marks UV absorbance at 280 nm. The fine dashed line marks UV absorbance at 254 nm. The course dashed line marks conductivity.

small leading shoulder contains contaminating host cell proteins. The first major peak, labeled AX1, is IgM. The last, labeled AX4, is DNA. The intermediate fractions AX2 and AX3 contain stable complexes. Entering peak-center 254:280 ratios into the Warburg plot (Fig. 1) showed that AX1–AX4 contained 1.0, 6.8, 69.4, and 100% DNA, respectively. Fraction AX2 contains what we refer to as IgM-dominant complexes. AX3 contains DNA-dominant complexes. Fig. 3 illustrates reduced SDS PAGE results. IgM heavy and light chains are apparent in both complex fractions, with minor bands indicating the presence of various protein contaminants (arrowheads). Note that no protein is visible in AX4.

Based on the aggressive precipitation when we combined purified DNA with purified IgM, we expected the complex to be dominated by large aggregates, with the largest ones containing the highest proportion of DNA. To the contrary, when sample pooled from AX2 and AX3 was applied to analytical SEC, about 75% of the complex (280 nm) was in a single peak with the same elution vol-

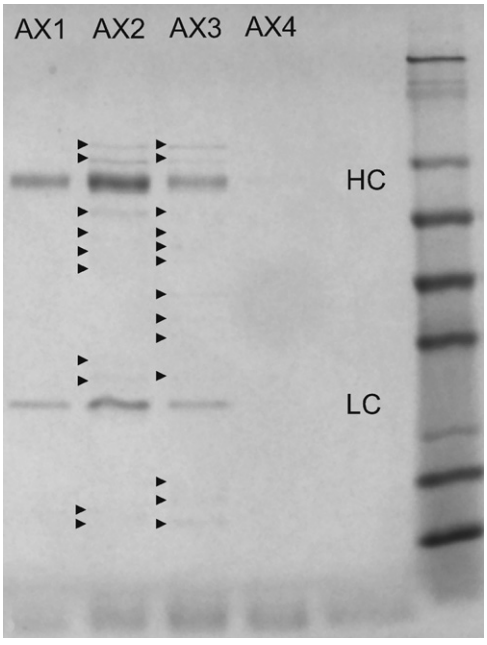

Fig. 3. Reduced SDS PAGE of anion exchange fractions from Fig. 2. The two dominant bands in fractions AX1–AX3 are IgM heavy and light chain. Trace protein contaminants are indicated by arrowheads.

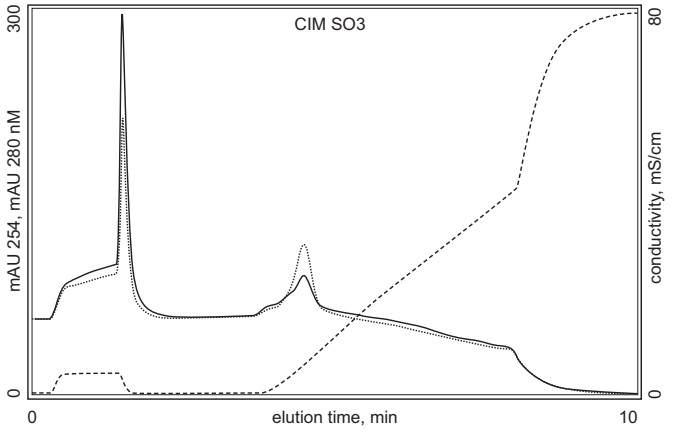

Fig. 4. Cation exchange of IgM:DNA complexes on CIM SO3 at pH 7.0. The solid black line marks UV absorbance at 280 nm. The fine dashed line marks UV absorbance at 254 nm. The course dashed line marks conductivity.

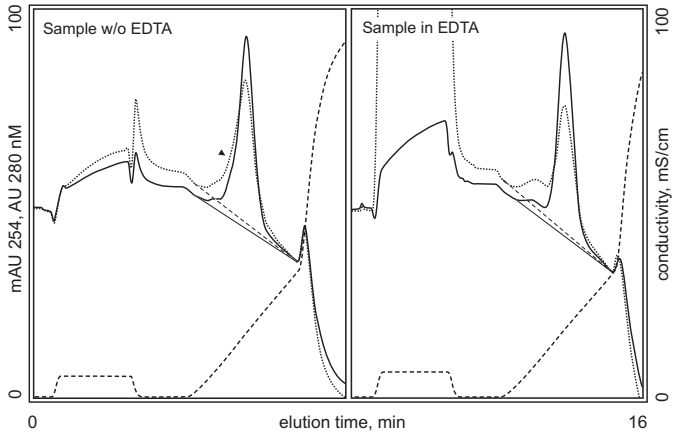

Fig. 5. Cation exchange of IgM:DNA complexes on CIM SO3 at pH 6.0, showing the effect of sample treatment with EDTA. The solid black line marks UV absorbance at 280 nm. The fine dashed line marks UV absorbance at 254 nm. The course dashed line marks conductivity. The arrowhead highlights a leading shoulder on untreated sample that is absent from the EDTA-treated sample.

ume as the DNA-depleted reference: 8.29 mL at peak center. IgM is usually a cyclic pentamer [20,23]; a disk with a hydrodynamic radius of about 20 nm [8]. Micro-BCA and qPCR indicated that the complex contained 700 μg/mL IgM and 167 μg/mL DNA, 24% of the IgM value. Using a molecular weight of 960 kDa for IgM, this indicated a total complex mass of about 1.19 MDa, with DNA contributing 229 kDa. Given an average molecular weight of 660 Da per base pair, this comes to an average of 347 base pairs of DNA per IgM molecule [24]. At 0.34 nm per base pair, this corresponds to a total length of 118 nm, or about 3 times the hydrodynamic diameter of IgM [8,25]. SEC elution thus indicated that complexed DNA was in the form of fragments no greater than about 115 base pairs. Such segments could lie across the pentamer disk without increasing its hydrodynamic diameter. The probability of such perfect alignment seems remote, so their size distribution is likely much smaller. Note also that SEC would be blind to DNA fragments complexed between the pentamer arms or extending perpendicularly from the diameter of the disk.

3.2. Cation exchange behavior of complexes

Cation exchangers should not bind DNA. They have the same charge, so DNA should be expelled immediately after injection. The presence of peaks with high 254 absorbance therefore indicates that any DNA present must be bound through an intermediate, in this case the IgM to which it is complexed. Fig. 4 is a chromatogram illustrating results from application of IgM:DNA complexes to a cation exchanger at pH 7. A large proportion of the sample was unretained. DNA-depleted IgM bound completely under these conditions (not shown). The high 254:280 ratio indicates that the unbound material is strongly DNA-dominant. An absorbance spike occurs at the end of the sample load, coinciding precisely with the conductivity reduction at the beginning of the wash. We have previously observed this pattern with other partially purified IgMs, and noted that the flow-through and wash spike do not occur with DNA-depleted IgM. We also note a published application showing CX capture of IgM directly from cell culture supernatant, where the accompanying PAGE gel shows a significant proportion of IgM in the flow-through, despite strong retention of the main antibody peak and the loss apparently not due to overloading [10].

3.2.1. Electrostatic complexes

We suggest that these failures to bind CX result from small DNA fragments blocking positive charge domains on the surface of the IgM, at least neutralizing the positive charges needed to bind CX, or potentially changing the local charge to negative and causing the complex to be repelled from the exchanger surface. According to this model, the absorbance spike at the end of the load would reflect increased charge repulsion between the exchanger and the IgM-bound DNA, caused by the reduction in conductivity. This model predicts that the end-of-load spike should be smaller at lower pH values where stronger positive charge on protein amino groups should weaken the repulsive influence of complexed DNA. Experimental data confirm this prediction (compare Fig. 4 with Fig. 5, first profile). As elution begins (Fig. 4), 254 absorbance becomes gradually less dominant, eventually crossing over and becoming inferior to the 280 trace. This is consistent with elution of a succession of increasingly IgM-dominant species. The species with the lowest 254:280 ratio elutes at the same position as DNA-depleted IgM (not shown), but it is not possible to be certain from the chromatogram that DNA has been entirely eliminated.

3.2.2. Metal-bridged complexes

Fig. 5 contrasts two CX chromatograms run at pH 6, the first similar to Fig. 4 except for the operating pH, the second similar to the first except that the sample was brought to 10 mM EDTA 60 minutes before it was injected. Note that EDTA itself absorbs UV; more at 254 than 280. This can be seen in the flow-through where its tetranegativity causes it to repelled by the column. Baseline offsets in the 254 and 280 profiles leave a less clear picture than Fig. 4, but several important differences are apparent: The main peak in the EDTA experiment lacks the leading shoulder seen in the control, it has higher 280 absorbance, and a lower 254:280 ratio. The Warburg value of the peak in the EDTA experiment is 2.6% DNA, versus 3.3% for the control. All these points suggest a degree of dissociation, but why should EDTA dissociate DNA:IgM complexes? It seems unlikely at 10 mM to disrupt strong electrostatic interactions. We suggest that the mechanism could be metal-bridging (IgM–metal–DNA). Proof of principle is found in the field of immobilized metal affinity chromatography. Many metals form strong coordination bonds simultaneously with dicarboxylic (immobilized iminodiacetic) acids and DNA phosphates [26]. Protein polycarboxy domains can bind divalent metal cations as effectively as iminodiacetic acid [9,27–29], creating the potential for protein-bound metal ions to simultaneously bind DNA phosphates. An important feature of metal coordination complexes is their ability to survive exposure to high salt concentrations. For example, both IgM and DNA bind HA calcium at 2 M NaCl in 10 mM phosphate [30,31]. This raises the important caution that metal

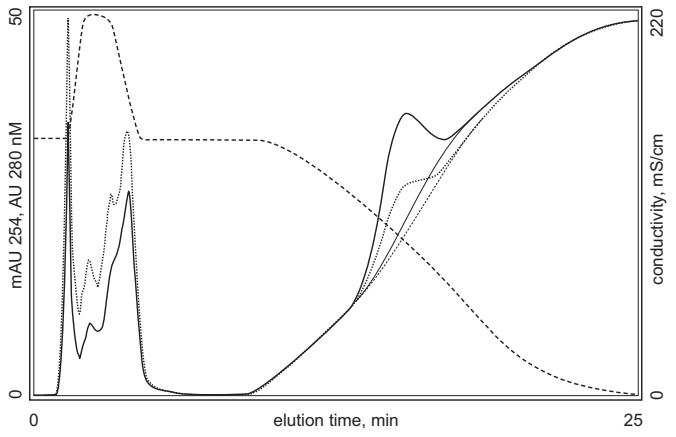

Fig. 6. Hydrophobic interaction chromatography of IgM:DNA complexes on PPG HW75. The solid black line marks UV absorbance at 280 nm. The fine dashed line marks UV absorbance at 254 nm. The course dashed line marks conductivity.

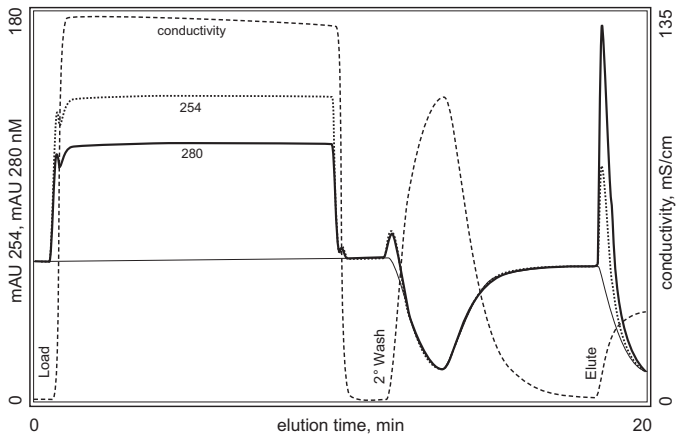

Fig. 7. Bioaffinity chromatography of IgM:DNA complexes on immobilized anti-lambda light chain camelid VHH. The solid black line marks UV absorbance at 280 nm. The fine dashed line marks UV absorbance at 254 nm. The course dashed line marks conductivity.

complexes can survive the conductivities encountered in all of the methods commonly used for protein purification.

IgM–metal–DNA complexes should be dissociated by EDTA. It also makes sense that such complexes would be configured in a distinctive way that would favor their binding to CX over electrostatically associated complexes, as observed in Fig. 5. Amino residues would be uninvolved and retain their full ability to bind CX. Involved IgM carboxyl clusters would be partially neutralized by the coordinated metal ion(s), thereby reducing local charge repellency to the cation exchanger. Any actual enhancement of CX binding would likely be swamped to a significant degree by the metal-bound DNA fragment, but the residual effect could be sufficient to explain the shoulder in the first profile and its elimination by EDTA in the second (Fig. 5). Since DNA-associated metal would bind different residues on the protein than DNA phosphates, DNA fragments could bind simultaneously by both mechanisms, each stabilizing the other. Metal-bridging could maintain protein:DNA complex integrity during exposure to high conductivity, and facilitate reformation of ionic bonds when conductivity was reduced; or ionic bonds could conserve complex integrity in the presence of EDTA at low conductivity. This highlights the potential value of dissociating complexes with multiple mechanisms when possible. Additional experimental work is required to evaluate metal-bridge complexes, but the fact that EDTA produces an observable difference of any kind provides adequate basis to suggest that metal affinity contributes to complex stability.

3.3. HIC behavior of complexes

Weak HIC ligands lack affinity for DNA, which should be eliminated upon injection. As with CX, the presence of elevated 254 absorbance in the bound fraction must therefore reflect binding through IgM. Fig. 6 is a chromatogram showing the results of complex application to a HIC column. It illustrates the same general response as CX, with DNA-dominant complexes flowing through the column upon sample application. Note the decreasing DNA content (254:280) across the flow-through. DNA content of the bound fraction appears be lower than on CX. This suggests that the high salt concentration in the sample may have dissociated some IgM-dominant complexes, but the pronounced asymmetry of the elution peak still suggests the presence of multiple species, and the 254:280 ratio across the peak indicates higher DNA content toward the leading side. The tip of the peak coincides with the elution position of DNA-depleted IgM, which produces a sharp narrow peak (not shown). As with CX however, it cannot be determined from the chromatogram if that portion of the peak in Fig. 6 is entirely free of DNA. More important is the fact that DNA-dominant complexes survived exposure to both 3.2 M sodium chloride, and 1.0 M ammonium sulfate. This invites speculation that high salt concentrations stabilize the complex in the same way that they promote IgM binding to the HIC support. Data addressing this point came from affinity chromatography experiments.

3.4. Affinity behavior of complexes

As with CX and HIC, DNA should not bind to bioaffinity media. Fig. 7 illustrates the second of a series of AC experiments in which IgM:DNA complexes were applied to the Lambda column at NaCl concentrations of about 300 mM, 1.5 M, and 3.0 M. The results were the same in every case: DNA-dominant complexes failed to bind. For this behavior to be consistent across this range of salt concentrations refutes the hypothesis that complexes were stabilized by high salt in the HIC experiment. In fact, the opposite appears to be true. The load for the second experiment was the flow-through from the first, with NaCl added to increase conductivity. The load for the third experiment was the flow-through from the second, with NaCl added. For there to have been a significant IgM elution peak in the second and third experiment means that the increasing salt levels must have promoted additional dissociation, not stabilized complexes.

The affinity column was washed before elution in each experiment with the urea–NaCl–EDTA buffer in the hope of fully dissociating the complexes and completely removing DNA. The wash always displaced a small 254-dominant peak (Fig. 7), but was never able to fully dissociate DNA (Fig. 8). This highlights the durability of complexes. On the positive side, IgM eluted from the affinity column had dramatically lower DNA content than the applied sample, and fairly consistent DNA content among experiments despite the highly variant NaCl concentrations of the feed streams. This suggests that even if DNA levels are variable from lot to lot coming out of cell culture, an affinity step could reproducibly reduce them to a level that could be managed adequately by appropriate downstream methods. However, comparison of Figs. 7 and 8 also raise an important caution about relying on 254:280 ratios. The 254:280 ratio of the affinity elution peak is 0.44, suggesting that it contains no DNA. The analytical AX profile reveals that this is not accurate. Fig. 8 also reveals that analytical CX is unable to discriminate low-level DNA contamination, and lends credence to the concern that preparative CX would suffer the same limitation.

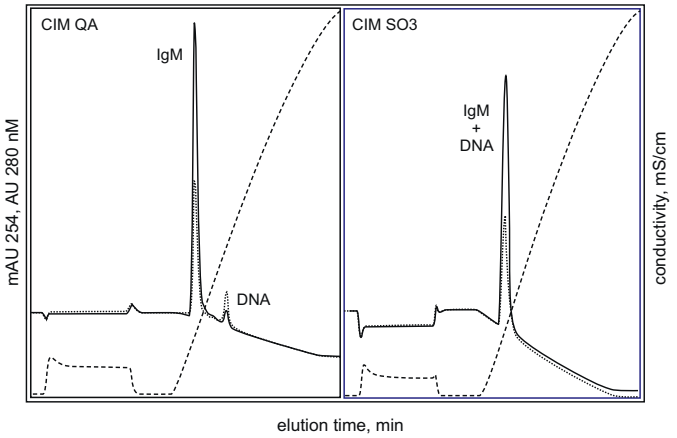

Fig. 8. Analytical anion exchange and cation exchange chromatography of the bioaffinity eluate on CIM QA and CIM SO3, both at pH 7.0. The solid black line marks UV absorbance at 280 nm. The fine dashed line marks UV absorbance at 254 nm. The course dashed line marks conductivity.

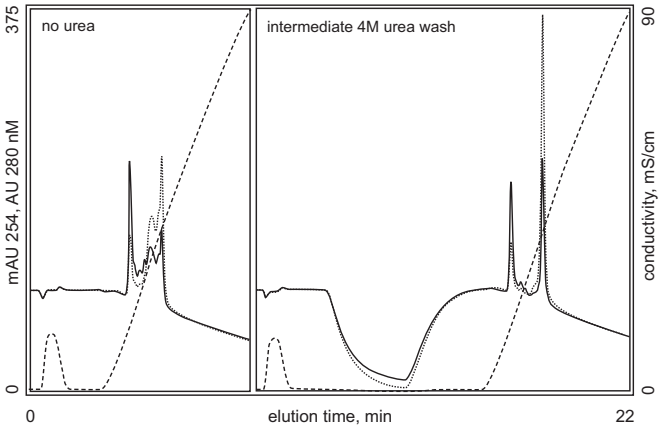

Fig. 10. Enhanced dissociation of IgM:DNA complexes on CIM QA following application of a pre-elution wash with 4 M urea. The solid black line marks UV absorbance at 280 nm. The fine dashed line marks UV absorbance at 254 nm. The course dashed line marks conductivity.

3.5. Anion exchange behavior of complexes

While AX on porous particles gave good fractionation of complexes from IgM and DNA (Fig. 2), it failed to support significant dissociation (Fig. 9). Monolithic anion exchangers however supported more effective dissociation than any other method, with CIM EDA offering better dissociation than CIM QA. Why does AX on monoliths support dramatically more effective dissociation than other methods? Tscheliessnig et al. suggested in reference to kinetic adsorption data that DNA might displace weaker binding IgM from AX [8]. This assumed however that DNA and IgM were behaving independently. We also believe strong DNA binding to monolithic AX is a key factor, but suggest that the densely charged exchanger surface simply outcompetes IgM for the DNA, thereby extracting DNA from the complex.

3.5.1. Enhancement of dissociation with mobile phase additives

If AX dissociates complexes by charge competition, additives that weaken complex integrity without weakening electrostatic interactions should enhance the process. Insertion of a pre-elution 4 M urea wash produced precisely this effect (Fig. 10). Urea is an effective hydrogen donor and acceptor, and it is nonionic [32]. It also weakens hydrophobic interactions, but given that such interactions between DNA and IgM seem not to be substantial, we suggest that it acts mainly through the former mechanism. Comparison with non-ionic or zwitterionic surfactants, or with organic solvents such as ethylene glycol, propylene glycol, alcohols, or others may provide additional insights. We also evaluated the effect of EDTA on AX but observed no detectable increase in dissociation. EDTA bound to the exchanger and eluted at the beginning of the NaCl gradient (not shown), suggesting that it was constrained from interacting with complexes.

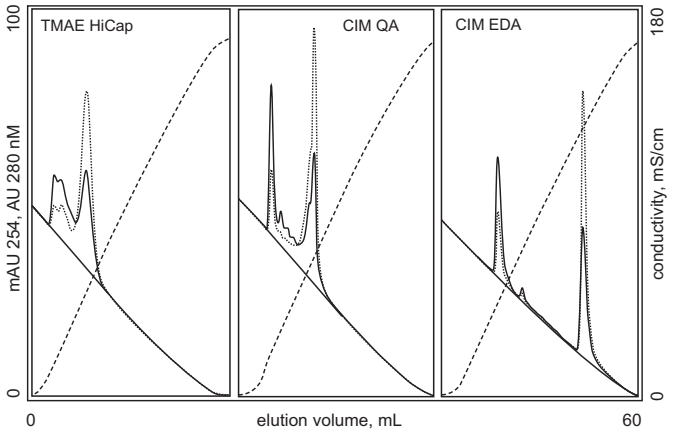

Fig. 9. Comparative anion exchange dissociation of IgM:DNA complexes on Fractogel TMAE HiCap, CIM QA, and CIM EDA. All experiments, 1 mL beds, 1 mL/min. The solid black line marks UV absorbance at 280 nm. The fine dashed line marks UV absorbance at 254 nm. The course dashed line marks conductivity.

3.5.2. Ligand and charge density

Why do monoliths support more effective complex dissociation than porous particles? Most discussions of relative DNA binding on porous particles and monoliths focus on the higher efficiency of convective mass transport in monoliths compared to diffusive transport in porous particles, but that argument rests on DNA being a very large molecule with a slow diffusion constant. In the present case, experimental results uniformly suggest that DNA fragments are small, so mass transport efficiency seems unlikely to be a significant factor. The higher ligand density of monoliths provides a compelling alternative. Ligand density on QA is reported at 0.9–1.1 mequiv./mL [33]. Ligand density on TMAE HiCap has been reported at 0.18–0.25 mequiv./mL [34]. Functional ligand density on TMAE HiCap may be even lower because exchange groups are distributed throughout the relatively deep layer of the tentacles, as opposed to monoliths, where exchange groups are understood to be restricted to the solid phase surface.

This leaves the question of why EDA supports more effective dissociation than QA. Ligand density on EDA is 60% higher (1.5–1.7 mequiv./mL) [35]. Besides that, EDA has two charged groups per ligand, giving it an actual charge density about 3 times higher than QA, and 12–15 times higher than TMAE HiCap. Elution conductivities reflect these trends generally, but not linearly (Table 1). DNA elution conductivity on QA was 22% higher than TMAE. DNA elution conductivity on EDA was 76% higher than QA and 115% higher than TMAE. Thus binding on EDA appears to be disproportionately strong, even considering its higher charge den-

Table 1
Elution conductivities of IgM and DNA from monolithic and porous particle anion exchangers at pH 7.0. All values in mS/cm at peak center.

	TMAE	CIM QA	CIM EDA
IgM	23.7	25.8	43.8
DNA	54.8	67.0	117.7

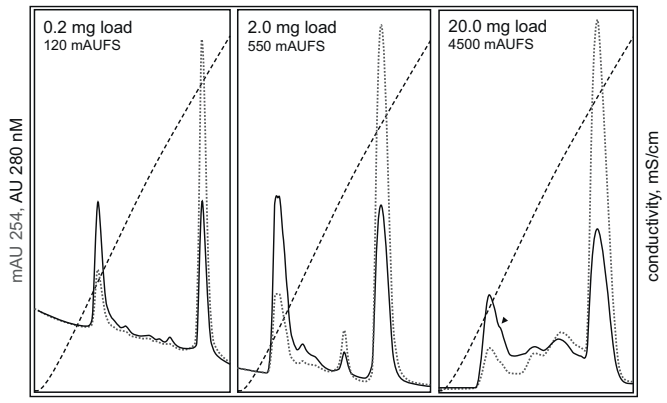

Fig. 11. Loss of dissociation efficiency with increasing complex load on CIM EDA (1 mL, 1 mL/min). The solid black line marks UV absorbance at 280 nm. The fine dashed line marks UV absorbance at 254 nm. The course dashed line marks conductivity.

sity, and suggests the additional contribution of a mechanism other than electrostatic attraction. Separate but related lines of evidence suggest that this mechanism is hydrogen bonding. EDA contains a primary and a secondary amino group [35]. AX ligands with lower degrees of substitution have stronger hydrogen bonding potential than fully substituted amines, and they bind DNA more strongly [36]. AX media that are chemically blocked to reduce hydrogen bonding potential bind DNA more weakly than their unblocked counterparts [37].

3.5.3. Dissociation capacity

Fig. 11 illustrates results with 0.2, 2.0, and 20.0 mg complex loads (expressed as IgM mass plus 24% to account for DNA) on a 1 mL triplet EDA monolith. Dissociation efficiency decays in proportion with the mass loaded. If DNA was able to displace IgM as suggested by Tscheliessnig et al. [8], we might have expected to see outstanding dissociation at all loads short of breakthrough; possibly even after. The fact that dissociation efficiency diminishes gradually with load suggests that as the exchanger surface becomes covered, already-bound DNA reduces the average charge potential on the surface of the exchanger, reducing its ability to dissociate newly introduced complexes. A similar hypothesis has been advanced to explain why IgG binding capacity goes down on cation exchangers under conditions that favor extremely high charge affinity between the antibody and the exchanger [38,39].

3.5.4. Dynamic binding capacity of IgM

The higher dissociation capacity of EDA invited the expectation that it might offer higher dynamic binding capacity for uncomplexed IgM as well. It did not (Table 2). Among experiments conducted at ~6 mS, QA gave substantially higher capacity at all pH values, with a maximum of 51 mg/mL at pH 7. EDA at 3 mS/cm, pH 7.0 supported 69 mg/mL but this is not a condition we would recommend. The IgM was barely soluble under these conditions and backpressure ascended throughout the experiment, nearly shutting the system down just before breakthrough occurred. This is arguably tolerable for preliminary characterization at lab scale, but our experience has been that such loading conditions are not scalable.

Table 2
Dynamic binding capacity of monoclonal IgM on monolithic and porous particle anion exchangers as a function of pH at a conductivity of 6 mS/cm. All values in mg/mL at 5% breakthrough.

	CIM QA	CIM EDA	TMAE
pH 6.0	29	21	13
pH 7.0	51	36[a]	–
pH 8.0	24	16	–

[a] Dynamic binding capacity EDA at 3 mS/cm, pH 7.0 was 69 mg/mL.

TMAE HiCap gave the lowest value of the three exchangers: 13 mg/mL at pH 6, versus 21 and 29 for EDA and QA, despite the feed stream residence time being 4 times longer on the TMAE. These results are consistent with publications reporting experimental data and providing a rationale for differential capacity as a function of solute size on porous particle and monolithic ion exchangers. In general, porous particles support higher dynamic binding capacities for small solutes. Capacity diminishes with increasing solute size, due to reduced efficiency of diffusive mass transfer associated with lower diffusion constants of larger solutes [40,41]. The diffusive limitation also causes capacity to drop with increasing flow rate. Experimental data further suggest that diffusive pore size should be at least 10 times larger than a given solute to avoid hindering diffusion [42]. This imposes an additional burden on large solutes such as IgM [8].

Monoliths generally support higher dynamic capacities for large solutes. Convective mass transfer is relatively unaffected by either solute size or flow rate [40,41]. Monoliths have lower surface area than porous particles, which accounts for their lower small-solute capacity, but the large convective channels impose no restrictions on large-solute access to the exchanger surface. Higher capacity of larger solutes reflects the fact that surface coverage is a square function while mass is related to volume, which is a cubic function [43]: the mass of bowling balls covering a tabletop is greater than the mass of marbles covering the same surface. Our data fit perfectly with those of Yamamoto [44]. IgM at 960 kDa gives lower capacity on porous particles than thyroglobulin at 670 kDa, and higher capacity on monoliths. Our data also agree well with capacity values reported for other monoclonal IgMs: 37–43 mg/mL on both AX and CX monoliths [10].

Capacity trends reported by Tscheliessnig et al. [8] were reversed from ours. They observed higher capacity on a porous particle anion exchanger than on the EDA monolith. They suggested that higher capacity on the porous particle media resulted from exchanger groups being grafted onto tentacles that enhanced their interactions with proteins in the mobile phase [8]. This implies that grafting overcomes the solute size/surface access relationship described by Etzel [43] and Yamamoto [44], and leaves the open question of why we did not observe higher capacity on TMAE. Unfortunately, there are too many unmatched variables among studies to support a coherent hypothesis. Future studies will hopefully resolve these discrepancies.

4. Conclusions

A baseline study was conducted to characterize naturally occurring IgM:DNA complexes and their chromatographic behavior. The majority of complexes were found to consist of single IgM molecules bound to small DNA fragments totaling about 24% of the overall complex mass. Complex integrity appears to be maintained primarily by electrostatic interactions between negatively charged DNA phosphates and positively charged protein amino groups, with secondary stabilization by hydrogen bonding and metal affinity. Complexes also contained numerous low-level protein contaminants that create potential for hydrophobic interactions to contribute additional stabilization.

Complexes exhibited a spectrum of chromatographic behaviors uncharacteristic of either IgM or DNA. DNA-dominant complexes were unretained by either bioaffinity or HIC, and repelled by CX. This behavior is generally consistent with expected behavior for DNA on these media, but subpopulations showed a degree of retar-

dation as they flowed through HIC and CX, illustrating the influence of the IgM component. IgM-dominant complexes were retained by all three methods, but HIC and CX showed prematurely eluting subpopulations, illustrating the influence of the DNA component. AX binds DNA more strongly than IgM. Complexes eluted as intermediate peaks on porous particle exchangers. Complexes were largely dissociated on monolithic exchangers. The difference between solid phase formats can be attributed to higher charge density on monoliths. The higher complex-dissociative efficiency of AX monoliths compared to other methods suggests that their high charge density outcompetes IgM for complexed DNA.

From a practical perspective, complexes impose novel strata of IgM and DNA heterogeneity that depress product recovery and reduce effectiveness of contaminant removal for every chromatographic method we investigated. This burden is compounded by the inclusion of host cell protein contaminants. Complexes become vehicles for protecting these contaminants from removal by fractionation methods that should reasonably be expected to remove them with ease. These burdens have obvious consequences for purification process development.

The complexation mechanisms revealed by this study are not limited to IgM. Any biological product with a strong positive charge domain is at risk of forming electrostatic complexes with DNA. Candidates particularly include IgG, a wide range of clotting factors, and virus particles for vaccine applications. Acidic proteins offer elevated potential for formation of metal complexes, which may be even more problematical since such complexes are expected to survive high conductivity environments. DNA plasmids are candidates for complexation with contaminating proteins by both mechanisms.

This study identifies several warning indicators. Monitoring chromatograms simultaneously at multiple wavelengths is effortless and provides a fair first approximation of relative DNA content. Unexpected product loss in the flow-through of AC, HIC, or CX is a good indicator. The large amount of UV-absorbing substances in cell culture supernatants make differential UV absorbance an unreliable indicator during sample application, but PAGE can reveal unbound product at any point in a process. Analytical AX on a monolith can dissociate and reveal DNA in flow-through or bound fractions from other methods. EDA monoliths offer the highest degree of dissociation and are more tolerant of high sample salt concentrations than other exchangers.

If substantial complexation is confirmed, pre-elution washes with dissociating agents may enhance DNA removal. Elevated conductivity can be used to weaken electrostatic interactions in conjunction with any method except ion exchange. Urea can be used to weaken hydrogen bonding in conjunction with any method except HIC. EDTA can be used to suspend metal affinity in conjunction with any method except AX.

Acknowledgements

Thanks to Van Nguyen and Aparna Roy for performing qPCR and micro-BCA on the complex. Thanks also to Missag Parshegian, Alois Jungbauer, Mookambeswaran Vijaylakshmi, Mark Etzel, Ales Podgornik, Milos Barut, Nika Lendero Krajnc, Christina Paril, Lee Olech, and Russ Frost for insightful questions and suggestions during development of the manuscript. Some of the data in this study were presented at the 4th International Monolith Symposium, Portoroz, Slovenia, May 29–June 2, 2010 [27].

References

[1] M. Bieber, C. Twist, N. Bhat, N. Teng, Pediatr. Blood Cancer 48 (2007) 380.
[2] R. R. Irie, S. O'Day, D. Morton, Cancer Immunol. Ther. 53 (2004) 110.
[3] Y. Azuma, Y. Ishikawa, S. Kawai, T. Tsunenari, H. Tsunoda, T. Igawas, et al., Clin. Cancer Res. 13 (2004) 2745.
[4] H. Vollmers, U. Zimmerman, V. Krenn, W. Timmerman, B. Illert, F. Hensel, et al., Oncol. Rep. 5 (1998) 549.
[5] L. Hedvika, M. Horn, A. Zuercher, M. Imboden, P. Durrer, M. Seiberling, M.R. Pokorny, C. Hammer, A. Lang, Antimicrob. Agents Chemother. 53 (8) (2009) 3442.
[6] Q. Yang, Vaccine 27 (9) (2009) 1287.
[7] J. Lee, A. Tscheliessnig, A. Chen, Y. Lee, G. Adduci, A. Choo, A. Jungbauer, J. Chromatogr. A 1216 (2009) 2683.
[8] A. Tscheliessnig, D. Ong, J. Lee, S. Pan, G. Satianegara, K. Schriebl, A. Choo, A. Jungbauer, J. Chromatogr. A 1216 (2009) 7851.
[9] P. Gagnon, Purification Tools for Monoclonal Antibodies, Validated Biosystems, Tucson, 2009.
[10] P. Gagnon, F. Hensel, R. Richieri, Biopharm. Int. (March (Suppl.)) (2008) 26.
[11] M. Ogris, S. Brunner, S. Schuller, R. Kircheis, E. Wagner, Gene Ther. 6 (4) (1999) 595.
[12] M. Abdullah, R. Davies, J. Hill, J. Chromatogr. A 347 (1985) 129.
[13] A. Shukla, P. Hinckley, Biotechnol. Progr. 24 (2008) 1115.
[14] K. Luhrs, D. Harris, S. Summers, M. Parseghian, J. Chromatogr. B 877 (2009) 1543.
[15] F. Hensel, P. Gagnon, An effective platform for purification of IgM monoclonal antibodies, in: Oral Presentation, 5th International Symposium on Hydroxyapatite, Rottach-Egern, Germany, October 11–14, 2009, http://www.validated.com/revalbio/pdffiles/Patrys.pdf.
[16] O. Warburg, J. Christian, Biochem. Z. 310 (1942) 384.
[17] A. Johnstone, A. Thorpe, Immunochemistry in Practice, 2nd ed., Blackwell Scientific Publications, Oxford, 1987.
[18] J. Glasel, Biotechniques 18 (1995) 62.
[19] K. Manchester, Biotechniques 19 (1995) 208.
[20] K. Manchester, Biotechniques 19 (1996) 968.
[21] W. Wilfinger, K. Mackey, P. Chomczynski, Biotechniques 22 (1997) 474.
[22] T. Arakawa, D. Ejima, T. Li, J. Philo, J. Pharm. Sci. 99 (4) (2009) 1674.
[23] D. Randall, L. King, R. Corely, Eur. J. Immunol. 20 (1990) 1971.
[24] R. Garrett, C. Grisham, Biochemistry, 4th ed., Brooks Cole, 2008, p. 26.
[25] J. Watson, T. Baker, S. Bell, A. Gann, M. Levine, R. Losick, Molecular Biology of the Gene, 5th ed., Pearson Benjamin, Cunningham, London, 2004 (Chapters 5 and 6).
[26] L. Tan, W.-B. Lai, C. Lee, D. Kim, W.-S. Cho, J. Chromatogr. A 1141 (2007) 151.
[27] M. Gorbunoff, Anal. Biochem. 136 (1984) 425.
[28] M. Gorbunoff, Anal. Biochem. 136 (1984) 433.
[29] M. Gorbunoff, S. Timasheff, Anal. Biochem. 136 (1984) 440.
[30] P. Gagnon, F. Hensel, S. Lee, S. Zaidi, IgM purification, the fine print, in: Oral Presentation, 4th International Monoliths Symposium, Portoroz, May 29–June 2, 2009, http://www.validated.com/revalbio/pdffiles/MSS10B.pdf.
[31] P. Gagnon, P. Ng, Bioprocess. Int. 3 (7) (2005) 52.
[32] W. Jencks, Catalysis in Chemistry and Enzymology, McGraw-Hill, New York, 1969, p. 323.
[33] BIA Separations, Publication PSIS-QAD-0105, 2008, http://www.biaseparations.com/pr/260/362/specific-information.
[34] E. Müller, Chem. Eng. Technol. 28 (11) (2005) 1295.
[35] BIA Separations, Publication PSIS-EDADiec-0106, 2008, http://www.biaseparations.com/pr/249/312/specific-information.
[36] P. Tainen, P.-E. Gustavsson, A. Lunglof, P.-O. Larsson, J. Chromatogr. A 1138 (2007) 84.
[37] M. Etzel, W. Riordan, J. Chromatogr. A 27 (2009) 2621.
[38] C. Harinarayan, J. Mueller, A. Lungloff, R. Fahrner, J. van Alstine, R. van Reis, Biotechnol. Bioeng. 95 (2002) 775.
[39] N. Fontes, R. van Reis, in: U. Gottschalk (Ed.), Process Scale Purification of Antibodies, J.T. Wiley and Sons, Hoboken, NJ, 2009, p. 203.
[40] R. Hahn, M. Panzer, E. Hansen, J. Mollerup, A. Jungbauer, Sep. Sci. Technol. 37 (7) (2002) 1545.
[41] A. Podgornik, A. Strancar, Biotechnol. Annu. Rev. 11 (2002) S281.
[42] A. Jungbauer, J. Chromatogr. A 1065 (2005) 3.
[43] M. Etzel, in: F. Svec, T. Tennikova (Eds.), Monolithic Materials, Elsevier, Amsterdam, 2003, p. 213.
[44] S. Yamamoto, Trans. IChemE 84 (C1) (2006) 72.